

MobileXNet: An Efficient Convolutional Neural Network for Monocular Depth Estimation

Xingshuai Dong, Matthew A. Garratt, *Senior Member, IEEE*, Sreenatha G. Anavatti, and Hussein A. Abbass, *Fellow, IEEE*

School of Engineering and Information Technology, University of New South Wales, Canberra, Australia.

Abstract—Depth is a vital piece of information for autonomous vehicles to perceive obstacles. Due to the relatively low price and small size of monocular cameras, depth estimation from a single RGB image has attracted great interest in the research community. In recent years, the application of Deep Neural Networks (DNNs) has significantly boosted the accuracy of monocular depth estimation (MDE). State-of-the-art methods are usually designed on top of complex and extremely deep network architectures, which require more computational resources and cannot run in real-time without using high-end GPUs. Although some researchers tried to accelerate the running speed, the accuracy of depth estimation is degraded because the compressed model does not represent images well. In addition, the inherent characteristic of the feature extractor used by the existing approaches results in severe spatial information loss in the produced feature maps, which also impairs the accuracy of depth estimation on small sized images. In this study, we are motivated to design a novel and efficient Convolutional Neural Network (CNN) that assembles two shallow encoder-decoder style subnetworks in succession to address these problems. In particular, we place our emphasis on the trade-off between the accuracy and speed of MDE. Extensive experiments have been conducted on the NYU depth v2, KITTI, Make3D and Unreal data sets. Compared with the state-of-the-art approaches which have an extremely deep and complex architecture, the proposed network not only achieves comparable performance but also runs at a much faster speed on a single, less powerful GPU.

Index terms— Monocular depth estimation, depth prediction, convolutional neural networks, encoder-decoder, autonomous vehicles.

I. INTRODUCTION

Autonomous vehicles have been extensively used in many applications, such as aerial surveillance, search and rescue. In order to safely operate in cluttered and unpredictable environments, these vehicles require a strong awareness of their operational surroundings, in particular, the ability to detect and avoid stationary or mobile obstacles [1], [2]. Depth estimation provides a geometry-independent paradigm in order to detect free, navigable space with the minimum safe distance. For the sake of obtaining depth information, most previous research depends on active sensors, such as LiDAR and the RGB-D cameras. However, these devices are bulky and energy consuming, which inhibit their deployment on limited payload platforms, for example, Micro Aerial Vehicles (MAVs). In contrast, monocular RGB cameras are lightweight and have low power consumption. More importantly, they provide richer information about the environment, which can be processed and applied in real-time. As a result, depth estimation from single RGB images has become a desirable alternative to active sensors.

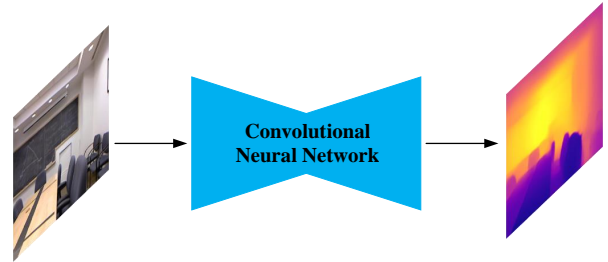


Fig. 1: The overall pipeline of CNN-based monocular depth estimation (best viewed in color).

State-of-the-art methods [3]–[10] normally utilize CNNs to learn features in order to predict a depth value for each pixel, and significantly outperform their classical counterparts [11]–[13]. However, these methods were developed based on extremely deep and complex network architectures. Therefore, they suffer a heavy computational cost and cannot be run in real-time without using high-end GPUs. Therefore, it is impractical to deploy those methods on platforms where reaction time is critical, such as small drones.

On the other hand, Wofk et al. [14] introduced an encoder-decoder network using the lightweight CNN [15]. Network pruning techniques [16] were used to further reduce the size of the model. Despite their method achieving a significant improvement in speed, the accuracy was not comparable to the state-of-the-art results.

In general, the above-mentioned methods employ the fully convolutional part of the CNNs [15], [17]–[19] designed for image classification as the feature extractor/encoder. However, these networks downsample the resolution of the final feature maps to $1/32$ scale of the input image. Although successive downsampling increases the receptive field and enables the generated feature maps to include more semantic information, it results in loss of spatial information. It is difficult to accurately recover this type of information from these feature maps. Hence, the accuracy of depth estimation will be impaired, in particular, when small sized images are processed. Moreover, the loss functions (i.e., the L_1 loss, L_2 loss and berHu loss) used by those methods are insensitive to the errors which occur at step edges. This leads to distorted and blurry edges in the estimated depth maps.

To address the above problems, we propose a novel CNN and a hybrid loss function for monocular depth estimation (MDE) in this study. Particularly, we aim to develop a network which has a proper trade-off between accuracy and speed. To be specific, the proposed network assembles two

relatively shallow encoder-decoder style subnetworks back-to-back in a unified framework. Compared with the previous studies [3]–[10], our network has a much shallower and simpler architecture as it is built on top of a series of simple convolutional layers rather than Inception modules [20] or Residual blocks [17]. In addition, each subnetwork involves less downsampling operations. This enables the intermediate feature maps to have a larger resolution and contain more spatial information, which is beneficial for depth estimation on small sized images. To the best of our knowledge, this work is the first attempt that stacks shallow encoder-decoder style CNNs in a unified framework to avoid the loss of spatial information and enhance the network’s representative ability for depth estimation. Different from existing work [5], [10], our method avoids the loss of spatial details but does not incorporate a separate spatial branch or fuse the hierarchical features of the encoder network. To preserve more edge details of objects, we design a hybrid loss function which adds constraints on the gradient data of depth maps.

Since the proposed network is designed for autonomous driving and mobile robots as well as is inspired by the XNet [21], we refer to it as “MobileXNet” in this paper. Compared with the XNet network, MobileXNet has three different characteristics. First, it is developed for the regression application rather than the classification task. In addition, the encoder of the first subnetwork consists of a series of depthwise separable convolutional layers [22], which enables a faster computational speed. Finally, a bridge module is inserted between the encoder and decoder in each subnetwork, including a set of dilated convolutional layers with different dilation rates, to capture the context information in multiple scales. This configuration generates better results than those derived using a single dilation rate. As a result, the proposed MobileXNet can be used for depth estimation in a faster and more effective manner in contrast to the XNet method.

The contributions of this study are summarized as follows: (1) We introduce a novel CNN architecture for achieving running efficient and accurate depth estimation from a single image; (2) We design a hybrid loss function; (3) We evaluate the proposed method on a dataset consisting of small sized synthetic images. In particular, we show that the size of the filters used in the input layer of CNNs has an influence on the performance of MDE when small sized images are processed; (4) We use Pareto Optimality to compare the error and running time over different methods, which has not been exploited in depth estimation; and (5) We demonstrate that the proposed method not only generates comparable accuracy to the state-of-the-art methods which use either extremely deep and complex architecture or post-processing but also runs much faster on a single less powerful GPU.

The rest of this paper is organized as follows. The related work is reviewed in Section II. In Section III, our methodology is introduced. The experimental setup and results are reported in Sections IV and V respectively. Finally, conclusions and future work are presented in Section VI.

II. RELATED WORK

In this section, we review the related works for monocular depth estimation. We categorize the reviewed methods

into traditional handcrafted feature-based methods and deep learning-based methods.

A. Traditional Handcrafted Feature-based Methods

Monocular depth estimation (MDE) has been an active research topic in the research community of computer vision and autonomous driving. The early works mainly depend on hand-crafted features and probabilistic graphical models. Saxena et al. [11] exploited the absolute and relative depth features and Markov Random Fields (MRF) to predict depth from monocular images. Later, the authors extended their work to 3D scene reconstruction [12]. Inspired by [12], Liu et al. [23] proposed a method which uses semantic labels as the contextual information for MDE. They use a learned MRF to infer the semantic class for each pixel, and then apply the L-BFGS algorithm to obtain a pixel-wise depth image.

In addition to the above mentioned parametric methods, MDE can also be solved as a non-parametric problem by inferring the whole depth map from candidate depth maps. Karsch et al. [13] introduced a pixel transfer-based method. Given an input image, they first search similar images from a dataset by matching GIST features. A set of possible depth values for the scene are constructed by applying label transfer between the given input image and the matched image. Liu et al. [24] designed a discrete-continuous conditional random field (CRF) to avoid the over-smoothing and maintain occlusion boundaries in the predicted depth maps.

The approaches described above all depend on handcrafted features to predict depth values. However, these features are designed beforehand to ‘describe’ a given set of chosen characteristics. As a result, they may fail when transferred to a new environment.

B. Deep Learning-based Methods

Motivated by the success of CNN in image classification, dense prediction tasks have also been addressed using CNN-based methods [2]–[10], [25]–[30]. Eigen et al. [25] introduced the first deep learning-based MDE method. Two deep networks were employed to fulfill the task, the first network predicts a global depth map from the entire image while the second network refines the global prediction at a local level. Eigen and Fergus [26] extended [25] to multi-task learning. Liu et al. [27] developed a deep convolutional neural field (DCNF) network. The designed DCNF combines the strength of deep CNN and continuous CRF in a unified framework. Both [25] and [27] use fully connected (FC) layers, which involve a huge number of parameters resulting in expensive computation.

To avoid the latency from FC layers, Laina et al. [3] proposed a fully convolutional residual network (FCRN) for MDE. FCRN consists of an encoder and a decoder. The encoder is built on the same basis as the fully convolutional part of ResNet-50, which produces feature maps at 1/32 scale of the input image. The decoder incorporates these feature maps and outputs the final depth map. Furthermore, Laina et al. demonstrated that the depth of the encoder network has great influence on the accuracy of depth estimation, because a deeper network has a larger receptive field. Inspired by this finding, [4], [5], [8]–[10] utilized CNNs have more than 100

layers in the encoder and produced much better results than their variant with ResNet-50 [17]. Besides, Hu et al. [8] and Chen et al. [9] also exploited multi-scale features and added a refinement module to their network.

Cao et al. [4] formulated depth estimation as a pixelwise classification task. In addition, fully connected CRFs are used as a post-processing operation to further improve the performance. Li et al. [5] used side-outputs from the different layers of encoder network to exploit multi-scale features for depth estimation. The above mentioned methods either build on top of the extremely deep CNNs [3], [5], [8], [9] or use post-processing operations [4]. Thus, they suffer a heavy computational cost and cannot be run in real-time without high-end GPUs.

To accelerate the running speed of MDE, Wofk et al. [14] designed an encoder-decoder network by using a lightweight CNN [15] as encoder. Moreover, they utilize network pruning techniques [16] to further reduce the model size. Although the obtained network has achieved great improvement in speed, the accuracy of depth estimation decreased significantly. Recently, Zhou et al. [28] designed a PADENet for panoramic monocular depth estimation. They trained the PADENet in unsupervised manner in order to overcome the lack of omnidirectional image dataset with groundtruth depth.

Motivated by the above mentioned approaches, in this study, we aim to develop a CNN which has a proper trade-off between the accuracy and speed of depth estimation. Specifically, we design the network by assembling two relatively shallow encoder-decoder style subnetworks in a unified framework but do not use any post-processing module. In addition, we build our network on top of a series of simple convolutional layers rather than Inception modules [20] or Residual blocks [17]. Benefiting from this design, our network has a simple and shallow architecture. Since the unsupervised learning methods normally suffer from lower accuracy, we trained the proposed network on datasets [12], [31]–[33] with the RGB images and ground-truth depth in a supervised fashion in order to acquire better accuracy.

III. METHODOLOGY

In this section, we first introduce the details of the proposed CNN architecture for monocular depth estimation (MDE) and then describe the loss functions used for training in this study.

A. CNN Architecture

Targeting at addressing the problems with state-of-the-art approaches and achieving the trade-off between accuracy and speed, we design a novel network which learns the end-to-end mapping from an RGB image to the corresponding depth map. We fulfil the task by assembling two simple and shallow encoder-decoder style subnetworks in a unified framework. As shown in Fig. 2b, each subnetwork only consist of simple convolutional layers. The encoder of the first subnetwork takes a single RGB image as input. After four times downsampling operation, it produces feature maps (F_1) at $1/16$ scale of the input image. This avoids a greater number of successive downsamplings which impairs the accuracy of recovering boundary level detail and the depth estimation on the small sized images. Subsequently, F_1 are passed through two up-sampling steps and the generated feature maps F_2 are fed to

the second subnetwork, which consists of two downsampling and four upsampling steps and outputs a dense depth map. In order to capture fine-grained image details, skip connections are applied to different levels of the designed network. Instead of concatenating, feature maps are fused via addition to avoid the increase of feature map channels processed in the decoder. This results in a further improvement in running speed.

To reduce network latency, we use depthwise separable convolution to design the encoder of the first subnetwork (see Fig. 2b). The depthwise separable convolution factorizes a regular convolution into a depthwise convolution and a pointwise convolution. Specifically, the depthwise convolution applies a single filter at each input channel, and the pointwise convolution is used to create a linear combination of the output of the depthwise layer.

The depthwise convolution with one filter per input channel is defined as:

$$\hat{G}_{k,l,m} = \sum_{i,j} \hat{K}_{i,j,m} \cdot F_{k+i-1,l+j+1,m}, \quad (1)$$

where \hat{K} is the depthwise convolutional kernel with size of $D_K \times D_K \times M$, and the m_{th} filter is operated on the m_{th} channel in F to produce the m_{th} channel of the output feature map \hat{G} . Hence, it has a computational complexity of $D_K \cdot D_K \cdot M \cdot D_F \cdot D_F$. Since the depthwise convolution only operates on input channels, and is followed by a 1×1 convolution which combines the output to generate the final feature map, the computational cost of depthwise separable convolutions is:

$$D_K \cdot D_K \cdot M \cdot D_F \cdot D_F + M \cdot N \cdot D_F \cdot D_F. \quad (2)$$

While for the regular convolution which has the same filter kernel size, the computation cost is $D_K \cdot D_K \cdot M \cdot N \cdot D_F \cdot D_F$. By using depthwise separable convolution we can reduce the number of parameters in convolutional layer to:

$$\frac{D_K \cdot D_K \cdot M \cdot D_F \cdot D_F + M \cdot N \cdot D_F \cdot D_F}{D_K \cdot D_K \cdot M \cdot N \cdot D_F \cdot D_F} = \frac{1}{N} + \frac{1}{D_K^2}. \quad (3)$$

For depthwise separable convolutions with kernel size of 3, the amount of computation is 8 to 9 times less than the regular convolution. Thus, it is helpful to improve the computation speed of MobileXNet. In order to take advantage of the pre-trained weights on the ImageNet dataset [34], we design the encoder (boxes with dotted line in Fig. 2b) of the first subnetwork with the same configuration as the first nine layers of MobileNet [15].

A larger receptive field enables the network to capture more context information, which can be leveraged to improve depth estimation performance [3]. The dilated convolution expands the receptive field of the neuron without increasing the number of model parameters [35]. Therefore, we insert a bridge module between the encoder and decoder in each subnetwork. Specifically, the bridge module consists of three dilated convolutional layers. Given a discrete function defined by $\mathcal{F} : \mathcal{Z}^2 \rightarrow \mathcal{R}$, let $\Omega_r = [-r, r]^2 \cap \mathcal{Z}^2$ and $k : \Omega_r \rightarrow \mathcal{R}$ be a discrete filter of size $(2r+1)^2$. The discrete convolution operator $*$ can be expressed as:

$$(F * k)(p) = \sum_{s+t=p} F(s)k(t). \quad (4)$$

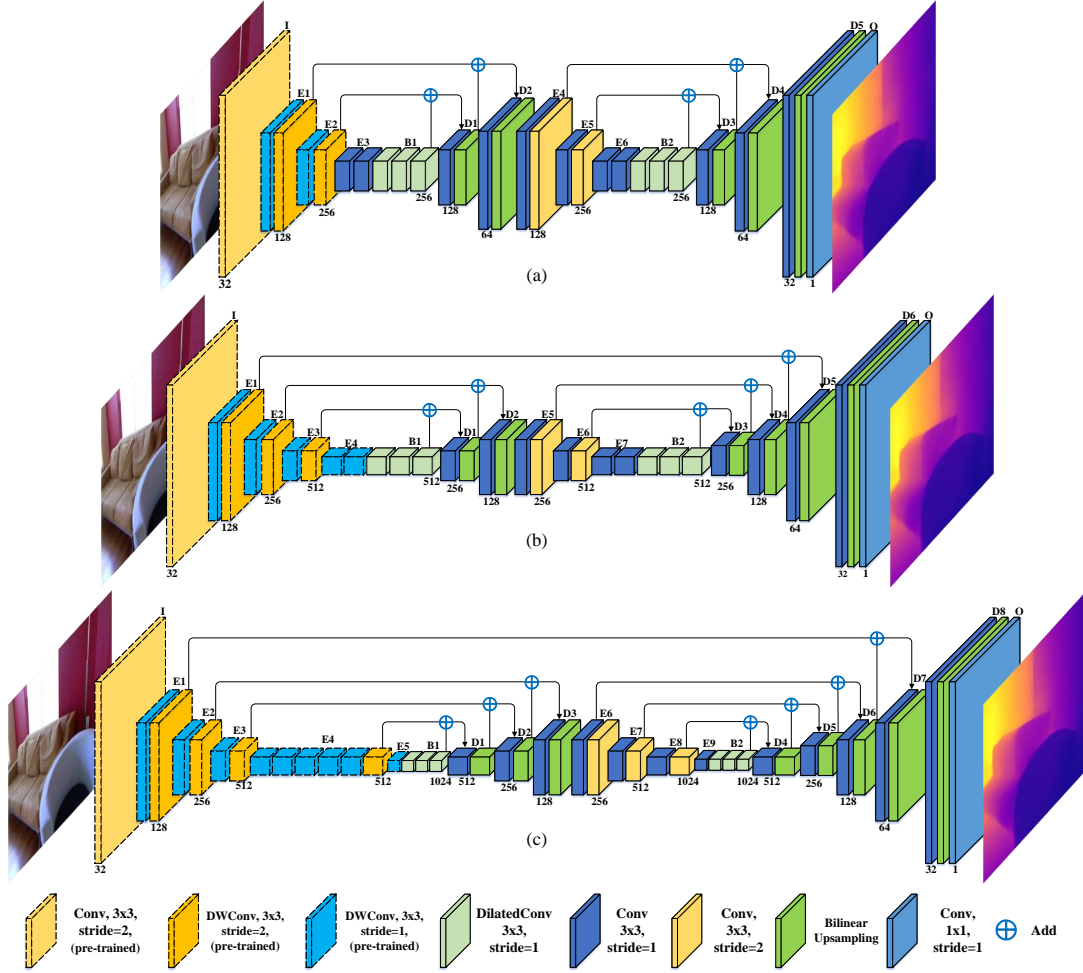


Fig. 2: Architecture of the proposed monocular depth estimation networks (best viewed in color). (a) MobileXNet-Small, (b) MobileXNet, and (c) MobileXNet-Large. I represents the input layer, E_i means the i_{th} encoder block, D_i indicates the i_{th} decoder block and O denotes the output layer.

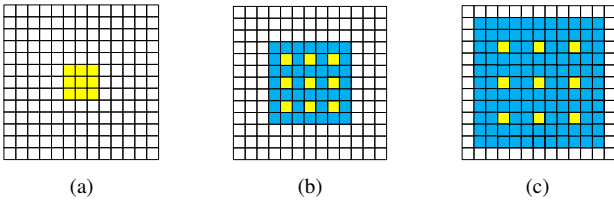


Fig. 3: Illustration of the dilated convolution. (a), (b), (c) are 1-dilated, 2-dilated, 3-dilated convolution respectively.

Based on this filter, the dilated convolution with a dilation factor r can be formulated as:

$$(F *_r k)(p) = \sum_{s+lt=p} F(s)k(t), \quad (5)$$

where $*_r$ is an r -dilated convolution. The regular convolution $*$ is simply the 1-dilated convolution. The illustration of dilated convolution is shown in Fig. 3. In this study, the dilation rates are set as 1, 2 and 3. By doing this, the decoders can get the context information captured in multiple scales.

The task of the decoder is to refine and upsample the output of the encoder. The core part of the decoder is the upsample layer, such as unpooling, up-projection, transpose

convolution and interpolation combined with convolution. According to [3], up-projection produced better performance than unpooling and transpose convolution. However due to the relatively complex architecture, it significantly increases the number of network parameters. Inspired by [36], we choose the combination of a bilinear interpolation and a 3×3 convolutional layer as the upsample layer in this study. The 3×3 convolutional layer reduces the number of output channels to half of the number of input channels. The bilinear interpolation increases the spatial resolution of intermediate feature maps to the same size as the output of the corresponding encoder layer. The main advantage of this design is the simple network architecture and reduced computational time.

We also design two variants that perform three and five times of downsampling in the first subnetwork, and we name them as MobileXNet-Small and MobileXNet-Large respectively. We train and test MobileXNet and the variants on the NYU depth v2 dataset [31] to compare the performance. The network architectures are shown in Fig. 2.

B. Loss Functions

A loss function is applied to measure how far the predicted depth map is from the groundtruth, and this is used to

supervise the update of network weights. Thus, it plays an important role in training CNNs. A commonly used loss function for depth estimation is the L_2 loss as it is more effective for pixels with larger error [37]. The L_2 loss is defined as:

$$L_2(d, d^*) = \frac{1}{N} \sum_i^N |d_i - d_i^*|^2, \quad (6)$$

where N is the number of pixels being considered, d and d^* are the predicted and groundtruth depth respectively. In [3], Laina et al. introduce a reverse Huber loss:

$$L_{berHu}(d, d^*) = \begin{cases} |d - d^*| & \text{if } |d - d^*| \leq c, \\ \frac{(d - d^*)^2 + c^2}{2c} & \text{otherwise,} \end{cases} \quad (7)$$

where c is the threshold and set as $c = \frac{1}{5} \max_i(|d - d^*|)$. The berHu loss is equal to L_2 loss when the error exceeds c , whilst when the error falls in $[-c, c]$ the berHu loss is equal to the mean absolute error (L_1 loss):

$$L_1(d, d^*) = \frac{1}{N} \sum_i^N |d_i - d_i^*|, \quad (8)$$

which is more robust to outliers in the dataset [38]. However, the above-mentioned loss functions are sensitive to errors emerging at step edges, such as difference between sharp and blurry edges [39]. To penalize the errors around edges, we define a hybrid loss which combines the regular L_1 loss with the image gradient-based L_1 loss:

$$L_{grad}(d, d^*) = \frac{1}{N} \sum_i^N |\nabla_x(d_i, d_i^*)| + |\nabla_y(d_i, d_i^*)|, \quad (9)$$

where ∇_x and ∇_y are spatial derivative in x and y direction respectively. Finally, the defined hybrid loss is formulated as:

$$L_{hybrid} = L_{depth} + L_{grad}, \quad (10)$$

where L_{depth} is the regular L_1 loss, and L_{grad} is the image gradient-based L_1 loss.

IV. EXPERIMENTAL SETUP

We introduce our experimental setup in this section. It includes three parts: implementation details, data augmentation methods and performance metrics.

A. Implementation Details

We implement the proposed networks using PyTorch. A desktop with an i7-7700 CPU, 16GB RAM and a single Nvidia GTX 1080 GPU is used for training and testing. The weights of the encoder of the first subnetwork of MobileXNet and its variants are initialized with the pre-trained weights. The other layers are initialized from the Gaussian distribution with a standard deviation of $\sqrt{2/N}$, where N represents the number of incoming nodes of one neuron. The training is optimized by using the SGD optimizer with an initial learning rate of 0.01, and the batch size is set as 8. For the NYU depth v2 [31], KITTI [32] and Unreal [33] dataset, we train the network for 20 epochs, and reduce the learning rate to 20% every 5 epochs. For the Make3D dataset [12], we train MobileXNet for 100 epochs, and reduce the learning rate to 20% every 40 epochs.

B. Data Augmentation

To increase the diversity of training samples, we utilize the following data augmentation methods, which are applied to each RGB and depth image pair in an online fashion:

- (1) Random rotation: RGB and depth image pairs are rotated by a random angle $r \in [-5, 5]$ degrees.
- (2) Random scale: RGB images are scaled by a random factor $s \in [1, 1.5]$, and the corresponding depth maps are divided by s .
- (3) Color Jitter: the brightness, contrast, and saturation of the RGB images are scaled by a random factor $c \in [0.6, 1.4]$.
- (4) Random flips: RGB and depth image pairs are horizontally flipped with the probability of 0.5.

C. Performance Metrics

In this work, we evaluate each method with the following metrics:

- (1) The Root Mean Square Error (RMSE):

$$RMSE = \sqrt{\frac{1}{N} \sum_i^N |d_i - d_i^*|^2}. \quad (11)$$

- (2) Mean Relative Error (REL):

$$REL = \frac{1}{N} \sum_i^N \frac{|d_i - d_i^*|}{d_i}. \quad (12)$$

- (3) Thresholded Accuracy (δ): it is the percentage of predicted pixels where the relative error is within a threshold. The formula is represented as follows:

$$\max\left(\frac{d^*}{d}, \frac{d}{d^*}\right) < \delta_i, \delta_i = 1.25^i. \quad (13)$$

- (4) Running time (t_{GPU}): the average execution time of testing each frame on a single GPU, we report the running time of our method on the GTX 1080 GPU. Due to the code and GPU model of some methods not being available to us, we cannot do a direct comparison on the Nvidia GPU. Therefore, we instead compare against their running time and GPU model as reported in the literature.

V. EXPERIMENTAL RESULTS

In this section, we present the experimental results on monocular depth estimation (MDE). We evaluate the proposed method on both indoor and outdoor scenes. Four data sets, the NYU depth v2 [31], KITTI [32], Make3D [12] and Unreal [33] are selected as benchmarks. Specifically, the NYU depth v2 dataset was captured in indoor environments, the KITTI [32] and Make3D dataset [12] were collected in real-world outdoor scenes, while the UnrealDataset [33] was gathered from simulated outdoor surroundings. We first evaluate MobileXNet with different loss functions and network configurations on the NYU depth v2 dataset [31]. Then, we compare it with state-of-the-art methods on four benchmarks.

TABLE I: Evaluation of loss functions (Rows 1-4) and dilation rates (Rows 4-8) on the NYU depth v2 dataset [31]. $[1, 2, 3]^*$ means depth-wise separable convolutions with dilations. The **red** and **bold** values indicate the best results.

Row	Method	Loss	Dilation Rates	RMSE	REL	δ_1	δ_2	δ_3	t_{GPU}
1	MobileXNet	\mathcal{L}_1	$[1, 2, 3]$	0.558	0.158	0.784	0.945	0.984	8.1 ms
2	MobileXNet	\mathcal{L}_2	$[1, 2, 3]$	0.553	0.158	0.777	0.948	0.986	7.8 ms
3	MobileXNet	berHu	$[1, 2, 3]$	0.550	0.160	0.779	0.947	0.987	8.9 ms
4	MobileXNet	Hybrid	$[1, 2, 3]$	0.537	0.146	0.799	0.951	0.988	7.9 ms
5	MobileXNet	Hybrid	$[1, 1, 1]$	0.552	0.156	0.785	0.946	0.985	6.8 ms
6	MobileXNet	Hybrid	$[2, 2, 2]$	0.545	0.156	0.794	0.947	0.987	9.0 ms
7	MobileXNet	Hybrid	$[3, 3, 3]$	0.533	0.148	0.797	0.951	0.987	8.9 ms
8	MobileXNet	Hybrid	$[1, 2, 3]^*$	0.552	0.162	0.786	0.942	0.984	6.2 ms
		Lower is better	Higher is better	$\delta_1 : \delta < 1.25, \delta_2 : \delta < 1.25^2, \delta_3 : \delta < 1.25^3$					

TABLE II: Evaluation of the weight initialization and convolution types in the encoder of the first sub-network (Rows 1-3) and the second sub-network (Rows 4-6) on the NYU depth v2 dataset [31]. DwConv indicates the depthwise separable convolutional layers initialized from the pre-trained weights, DwConv-IG represents the depthwise separable convolutional layers initialized from the Gaussian distribution, and Conv-IG means the regular convolutional layers initialized from the Gaussian distribution. The **red** and **bold** values indicate the best results.

Row	Method	Convolution Types	RMSE	REL	δ_1	δ_2	δ_3	t_{GPU}
1	MobileXNet	DwConv	0.537	0.146	0.799	0.951	0.988	7.9 ms
2	MobileXNet	DwConv-IG	0.669	0.198	0.692	0.909	0.973	8.5 ms
3	MobileXNet	Conv-IG	0.632	0.186	0.724	0.923	0.976	9.3 ms
4	MobileXNet	DwConv	0.822	0.209	0.584	0.862	0.961	6.8 ms
5	MobileXNet	DwConv-IG	0.550	0.156	0.788	0.947	0.986	7.3 ms
6	MobileXNet	Conv-IG	0.537	0.146	0.799	0.951	0.988	7.9 ms
Lower is better		Higher is better	$\delta_1 : \delta < 1.25, \delta_2 : \delta < 1.25^2, \delta_3 : \delta < 1.25^3$					

A. NYU Depth Dataset

The NYU depth v2 dataset [31] consists of about 240k RGB and depth image pairs captured from 464 different indoor scenes through a Microsoft Kinect camera. In this study, we train the designed method on about 48k synchronized RGB and depth images pairs, and test it on 654 images. Both training and testing data are released by [14]. Following [3], [14], [25], we first downsample the original images from 640×480 pixels to half size, and then center crop 304×228 pixels region as input to the network.

1) *Evaluation of Loss Functions*: In this subsection, we perform a set of experiments over different loss functions based on the designed MobileXNet. Four loss functions described in Section III-B are tested, and the results are listed in the first 4 rows of Table I. It can be observed that both the berHu loss and the L_2 loss outperform the L_1 loss. In addition, the berHu loss performs slightly better than the L_2 loss. It should be noted that the designed hybrid loss which combines the regular L_1 loss with the image gradient-based L_1 loss generates the best performance. Therefore, we use the hybrid loss function as the default loss in this study.

2) *Evaluation of Dilation Rate*: In this subsection, we evaluate the performance of different dilation rate configurations in the bridge modules. The dilation rates in the bridge modules are set as $[1, 1, 1]$, $[2, 2, 2]$, $[3, 3, 3]$ and $[1, 2, 3]$, while $[1, 1, 1]$ means the bridge modules have three regular convolutional layers. The results produced from these 4 configurations are listed in Rows 4 to 7 of Table I.

As can be seen, (1) the dilated convolutions improve the performance in both accuracy and error metrics. We attribute this to the fact that it has a larger receptive field and captures

more context information. It should be noted that we do not further increase the dilation rate, as we did not obtain empirical improvement when dilation rate was larger than 3; (2) the configuration of $[3, 3, 3]$ produces the best RMSE value, while the values of REL, δ_1 , δ_3 and running time are inferior to $[1, 2, 3]$. It demonstrates that using multiple dilated convolutional layers with different dilation rates to capture the multiple-scale context information is helpful in improving accuracy. Besides, the MobileXNet using the bridge modules with dilation rates of $[1, 2, 3]$ runs faster than $[3, 3, 3]$ by 1ms. This suggests that $[1, 2, 3]$ achieves better accuracy and speed balance; (3) we further apply depthwise separable convolutions with dilation rates of 1, 2 and 3 to the bridge modules. According to the 4th and 8th rows of Table I, the depthwise separable convolution lowers the running time by 1.7ms but the performance also decreased. However, the MobileXNet using the regular convolutions with dilation rates of $[1, 2, 3]$ generates the best performance and adequate speed for real-time application. Thus, we choose it as the default configuration.

3) *Effect of Weight Initialization*: To evaluate the effect of weight initialization in the backbone (the **encoder** of the **first** subnetwork) of MobileXNet, we initialized it with the pre-trained MobileNet model (row 1, Table II) and Gaussian distribution (row 2, Table II) respectively. Furthermore, we design a variant of MobileXNet by replacing the depthwise separable convolutional layers in the backbone with regular convolutional layers (row 3, Table II). Since the ImageNet dataset pre-trained weights of the regular convolutional layers are not available, we initialize them from the Gaussian distribution. As can be observed from the 2nd and 3rd rows

TABLE III: Comparison of the proposed MobileXNet against different variants and U-Net [40] on the NYU depth v2 dataset [31]. \triangle represents the first 9 layers of MobileNet, \square denotes the first 7 layers of MobileNet, \diamond means the network does not use CNN designed for image classification. M and G indicate $\times 10^6$ and $\times 10^9$ respectively. The **red** and **bold** values indicate the best results.

Row	Method	Backbone	Parameters	Flops	Memory	RMSE	REL	δ_1	δ_2	δ_3	t_{GPU}
1	MobileXNet	\triangle	24.95 M	9.78 G	111.12 MB	0.537	0.146	0.799	0.951	0.988	7.9 ms
2	MobileXNet-Small	\square	6.51 M	8.34 G	104.61 MB	0.606	0.180	0.733	0.930	0.981	6.1 ms
3	MobileXNet-Large	MobileNet	91.07 M	11.85 G	121.17 MB	0.538	0.148	0.799	0.952	0.987	15.2 ms
4	ShuffleXNet	ShuffleNetV2	5.20 M	1.73 G	41.93 MB	0.580	0.163	0.766	0.943	0.985	6.9 ms
5	EfficientXNet	EfficientNet-B0	1.96 M	0.39 G	74.19 MB	0.575	0.162	0.766	0.946	0.985	8.2 ms
6	U-Net [40] (Bilinear)	\diamond	17.27 M	42.22 G	401.05 MB	0.705	0.206	0.661	0.900	0.972	14.1 ms
7	U-Net [40] (DeConv)	\diamond	31.04 M	48.55 G	426.32 MB	0.726	0.212	0.644	0.892	0.971	19.8 ms
		Lower is better	Higher is better	$\delta_1 : \delta < 1.25, \delta_2 : \delta < 1.25^2, \delta_3 : \delta < 1.25^3$							

of Table II, when initialized from the Gaussian distribution, the variant with regular convolutional layers (row 3, Table II) outperforms the Gaussian distribution initialized MobileXNet (row 2, Table II) in RMSE, REL, δ_1 , δ_2 and δ_3 , while the running speed is inferior. We attribute this to the fact that the regular convolution has more parameters than the depthwise separable convolution. However, when initializing the backbone from the pre-trained weights (row 1, Table II), the performance of MobileXNet improved significantly. Thus, we choose the depthwise separable convolution in the backbone and initialize it from the pre-trained weights in this study.

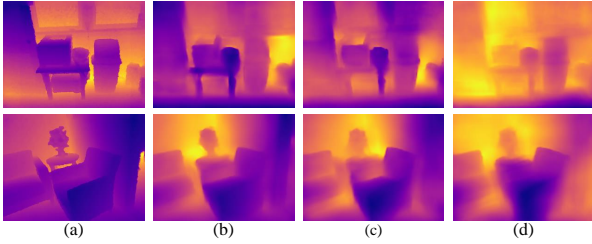


Fig. 4: Qualitative results of MobileXNet with different weight initialization and convolution type in the encoder of the second sub-network. (a) Groundtruth, (b) Conv-IG, (c) DWConv-IG, and (d) DWConv. Color represents depth (yellow is far, blue is close).

With the backbone initialized from the pre-trained MobileNet model, we further design the **encoder** of the **second** subnetwork (E5-E7 blocks in Fig. 2b) with depthwise separable convolutional layers and initialize it with the pre-trained weights of the corresponding layers of MobileNet [15]. Experimental results are shown in rows 4 to 6 of Table II. Figure 4 also displays the qualitative results.

It can be seen from Table II that when we initialized the encoder of the second subnetwork with the pre-trained weights (row 4, Table II), MobileXNet does not provide good performance. Furthermore, the produced depth maps are blurry and suffer from sharp discontinuities of shapes of objects (see Fig. 4d). We attribute the bad performance to the following facts. In essence, the MobileXNet stacks two encoder-decoder style sub-networks. The encoder and decoder of the first sub-network are trained to describe input images and generate feature maps with 1/4 size of the input image, respectively. The produced feature maps are passed

to the second subnetwork in order to produce depth maps. The second subnetwork works as a learned refining module which operates with downsampling and upsampling steps. This subnetwork tends to be more dependent on the training dataset than the backbone which is utilized to learn generic features [41]. The ImageNet dataset [34] used for pre-training the MobileNet is different from the NYU depth v2 dataset. Hence, initializing the encoder of the second subnetwork impairs the performance of depth estimation.

To further augment our experiments, we then initialize the parameters of the depthwise separable convolutional layers in the encoder of the second subnetwork with a Gaussian distribution (row 5, Table II). As shown in Table II, initializing the encoder of the second subnetwork from the Gaussian distribution outperforms initialization from pre-trained weights. Compared with the original MobileXNet (row 6, Table II), the MobileXNet with the depthwise separable convolution in the encoder of the second subnetwork has inferior performance. In addition, the boundary of small or thin objects in the produced depth maps (Fig. 4c) are unclear. Therefore, we use regular convolutional layers in the encoder of the second subnetwork and initialize it from the Gaussian distribution.

4) *Evaluation of Network Architectures*: To validate the effectiveness of the MobileXNet, we compare it with different variants. In addition to the MobileXNet-Small and MobileXNet-Large, we build two variants based on the ShuffleNetV2 [45] and EfficientNet [46] backbones. The corresponding variants are named as ShuffleXNet¹ and EfficientXNet² respectively. The standard encoder-decoder network, U-Net, is used as the baseline. Unlike [40], the U-Net includes batch normalization in this work. All methods were trained with the hybrid loss. The experimental results are shown in Table III.

It can be observed that: (1) among all methods, the MobileXNet generates the best error and accuracy metric results and its running time is only inferior to the fastest method by 1.8ms; (2) regarding the RMSE, REL, δ_1 , δ_2 and δ_3 metrics, the performance of MobileXNet-Large is very close to MobileXNet. However, due to its deep network architecture, the running time is almost doubled; (3) the MobileXNet-Small yields the fastest speed, while its error and accuracy metric results are inferior to its counterparts

¹The conv1 to stage 3 layers of ShuffleNetV2-1x [45] are used as backbone

²The stage 1 to stage 6 layers of EfficientNet-B0 [46] are used as backbone

TABLE IV: Comparison of performances on the NYU depth v2 dataset [31]. \diamond means the network does not use CNN designed for image classification, \triangle represents the first 9 layers of MobileNet. The **red** and **bold** values indicate the best results.

Row	Method	Backbone	RMSE	REL	δ_1	δ_2	δ_3	t_{GPU}	Device
1	Eigen et al. [25]	\diamond	0.907	0.215	0.611	0.887	0.971	N/A	N/A
2	Eigen and Fergus [26]	VGG-16	0.641	0.158	0.769	0.950	0.988	N/A	N/A
3	Liu et al. [27]	VGG-16	0.759	0.213	0.650	0.906	0.976	N/A	N/A
4	Laina et al. [3] (UpConv)	ResNet-50	0.604	0.132	0.789	0.946	0.986	78 ms	Nvidia GTX Titan
5	Laina et al. [3] (UpProj)	ResNet-50	0.573	0.127	0.811	0.953	0.988	55 ms	Nvidia GTX Titan
6	Cao et al. [4]	ResNet-152	0.540	0.141	0.819	0.965	0.992	N/A	N/A
7	Li et al. [5]	ResNet-50	0.601	0.147	0.808	0.957	0.985	N/A	N/A
8	He et al. [42]	VGG-16	0.572	0.151	0.789	0.948	0.986	N/A	N/A
9	Xu et al. [6]	ResNet-50	0.593	0.125	0.806	0.952	0.986	150	Nvidia Titan-X
10	Wofk et al. [14] (Original)	MobileNet	0.579	0.164	0.772	0.938	0.982	5.0 ms	Nvidia GTX 1080
11	Wofk et al. [14] (Final)	MobileNet	0.604	0.165	0.771	0.937	0.980	4.0 ms	Nvidia GTX 1080
12	Yang et al. [1]	ResNet-18	0.628	0.199	0.708	0.916	0.975	10 ms	Nvidia Titan-X
13	Hambarde and Murala [43]	\diamond	0.543	0.160	0.773	0.959	0.989	N/A	N/A
14	Spek et al. [44]	ERFNet	0.687	0.190	0.704	0.917	0.977	3.2 ms	Nvidia GTX 1080Ti
15	MobileXNet (Ours)	\triangle	0.537	0.146	0.799	0.951	0.988	7.9 ms	Nvidia GTX 1080
Lower is better			Higher is better	$\delta_1 : \delta < 1.25, \delta_2 : \delta < 1.25^2, \delta_3 : \delta < 1.25^3$					

except the U-Net [40]; (4) the network parameters, flops and memory footprint of ShuffleXNet are about $4\times$, $5\times$ and $2\times$ fewer than MobileXNet, but it only faster than MobileXNet by 1ms. Moreover, the performance of ShuffleXNet with respect to the error and accuracy metrics is not comparable to MobileXNet; 5) the EfficientXNet is optimal in terms of network parameters and flops, while its running time is longer than MobileXNet. This should be attributed to the fact that the EfficientXNet is built on top of EfficientNet [46], which is optimized for parameter and flops efficiency. Furthermore, EfficientNet scales the feature map resolution and depth at the same time, this leads to the slow GPU inference time [47]; and (6) the performance of U-Net [40] is inferior, no matter which upsampling method is used. In addition, it is the slowest especially when using transpose convolution (DeConv) for upsampling. It should be noted that the weights of U-Net are initialized from a Gaussian distribution.

The MobileXNet generates the best performance in terms of error and accuracy metrics and achieves real-time speed about 126 fps on a GTX 1080 GPU, which is adequate for autonomous driving and robotic applications. In this context, we choose MobileXNet as the network in this study. In the following part we compare its performance with the state-of-the-art.

TABLE V: Comparison of performance with respect to the benefit of data augmentation. The **red** and **bold** values indicate the best results.

Training Data	RMSE	REL	δ_1	δ_2	δ_3
Original	0.555	0.158	0.782	0.946	0.985
Augmented	0.537	0.146	0.799	0.951	0.988
Lower is better		Higher is better			

5) *Effect of Data Augmentation*: We employ data augmentation to increase the diversity of the training data to enable the trained network to have a better depth estimation performance. We train our MobileXNet on the original training data and the training data with online data augmentation to analyze the benefit of data augmentation. The standard 654 testing

images are used as testing data. Experimental results are listed in the last two rows of Table V. It can be observed that data augmentation improves the monocular depth estimation performance, especially the RMSE, REL and δ_1 metrics. Hence, we use data augmentation in this study.

6) *Comparison with the State-of-the-Art*: In this subsection, we compare MobileXNet with state-of-the-art methods [1], [3]–[6], [14], [25]–[27], [42]–[44]. Since we focus on depth estimation from single RGB images, thus, methods that fuse sparse depth points are not compared in this study. The results of [1], [3]–[6], [25]–[27], [42]–[44] are reported in respective literatures. While Wofk et al. [14] only report the values of RMSE and δ_1 , we run their released code and models on our desktop to get the values of REL, δ_2 , δ_3 and the running time on the GTX 1080 GPU. Table IV reports all experimental results.

As can be seen, MobileXNet performs much better than Spek et al. [44] in both error and accuracy metrics, and it generates the best RMSE result. Regarding REL, δ_1 , δ_2 and δ_3 metrics, MobileXNet also outperforms [1], [14], [26], [27], [42], [43]. In addition, the REL, δ_1 , δ_2 and δ_3 values of MobileXNet are on par with [3]–[6]. Compared with these four methods, MobileXNet has a shallow and simple architecture, which consists of significantly less layers. Specifically, MobileXNet uses the first 9 layers of MobileNet as backbone, which is much shallower than the ResNet-50 and ResNet-152 utilized by [3]–[6]. Regarding the decoder network, our upsample layer consists of a 3×3 convolutional layer and bilinear interpolation, while Laina et al. [3] (UpProj) utilizes a relatively complex Up-projection method. In addition, [5] and [6] integrate multi-scale side output feature maps and [4] uses CRF as post-processing operation.

It can be observed from Table IV that Spek et al. [44] yields the fastest running speed, while it performs worse than most of the counterparts in terms of the accuracy and error metrics. Our MobileXNet runs slightly slower than Wofk et al. [14], which is tested at 224×224 sized images. It should be noted that the MobileXNet runs on images having 228×304 pixels. The running speed of MobileXNet is significantly

TABLE VI: Comparison of performances on the KITTI Eigen-split [25]. \diamond means the network does not use CNN designed for image classification, \triangle represents the first 9 layers of MobileNet. The **red** and **bold** values indicate the best results.

Row	Method	Cap	Backbone	RMSE	REL	δ_1	δ_2	δ_3	t_{GPU}	Device
1	Eigen et al. [25]	80 m	\diamond	7.156	0.190	0.692	0.899	0.967	N/A	N/A
2	Liu et al. [27]	80 m	VGG-16	6.986	0.217	0.647	0.882	0.961	N/A	N/A
3	Cao et al. [4]	80 m	ResNet-152	4.712	0.115	0.887	0.963	0.982	N/A	N/A
4	Godard et al. [48]	80 m	VGG-16	5.927	0.148	0.803	0.922	0.964	35 ms	Nvidia Titan-X
5	Zhou et al. [49]	80 m	\diamond	6.856	0.208	0.678	0.885	0.957	30 ms	Nvidia Titan-X
6	Li et al. [5]	80 m	ResNet-50	5.325	0.128	0.833	0.956	0.985	N/A	N/A
7	Poggi et al. [50]	80 m	\diamond	5.907	0.146	0.801	0.926	0.967	20 ms	Nvidia Titan-X
8	Casser et al. [51]	80 m	\diamond	5.521	0.142	0.820	0.942	0.976	34 ms	Nvidia GTX 1080Ti
9	Yusiong and Naval [52]	80 m	\diamond	5.909	0.145	0.824	0.936	0.970	160 ms	Nvidia GTX 1080Ti
10	Eom et al. [2]	80 m	\diamond	4.537	0.117	0.865	0.958	0.983	130 ms	Nvidia Titan-X
11	Hambarde and Murala [43]	80 m	\diamond	5.285	0.142	0.797	0.932	0.975	N/A	N/A
12	Liu et al. [53]	80 m	\diamond	5.264	0.141	0.825	0.941	0.976	18.57 ms	Nvidia GTX 1080Ti
13	Ye et al. [10]	80 m	ResNet-101	4.978	0.112	0.842	0.947	0.973	N/A	N/A
14	MobileXNet (Ours)	80 m	\triangle	4.965	0.103	0.873	0.959	0.985	15.4 ms	Nvidia GTX 1080
15	Cao et al. [4]	50 m	ResNet-152	3.605	0.107	0.898	0.966	0.984	N/A	N/A
16	Godard et al. [48]	50 m	VGG-16	4.471	0.140	0.818	0.931	0.969	35 ms	Nvidia Titan-X
17	Zhou et al. [49]	50 m	\diamond	5.181	0.201	0.696	0.900	0.966	30 ms	Nvidia Titan-X
18	Poggi et al. [50]	50 m	\diamond	4.608	0.145	0.813	0.934	0.972	20 ms	Nvidia Titan-X
19	Yusiong and Naval [52]	50 m	\diamond	4.014	0.122	0.864	0.953	0.978	160 ms	Nvidia GTX 1080Ti
20	Eom et al. [2]	50 m	\diamond	3.493	0.113	0.877	0.963	0.985	130 ms	Nvidia Titan-X
21	Liu et al. [53]	50 m	\diamond	4.067	0.135	0.838	0.947	0.978	18.57 ms	Nvidia GTX 1080Ti
22	Spek et al. [44]	50 m	ERFNet	4.363	0.156	0.818	0.940	0.977	3.2 ms	Nvidia GTX 1080Ti
23	MobileXNet (Ours)	50 m	\triangle	3.842	0.098	0.886	0.966	0.987	15.4 ms	Nvidia GTX 1080

Lower is better Higher is better $\delta_1 : \delta < 1.25$, $\delta_2 : \delta < 1.25^2$, $\delta_3 : \delta < 1.25^3$

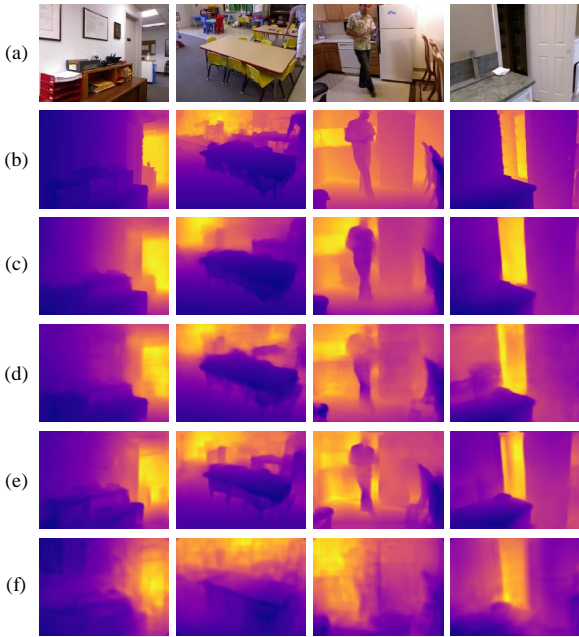


Fig. 5: Qualitative comparison on the NYU depth v2 dataset. (a) RGB, (b) Groundtruth, (c) Our results, (d) Wofk et al. [14] (Final), (e) Eigen and Fergus [26], and (f) Eigen et al. [25] (Fine). Color represents depth (yellow is far, blue is close).

faster (7.9ms vs 150ms) than Xu et al. [6], which was tested on a Titan-X GPU. While the running time is obtained with different GPUs, the Titan-X GPU has 3584 CUDA cores and 12GB memory, which is much stronger than our 1080 GPU

(2580 CUDA cores and 8GB memory). With the same sized images, the speed of MobileXNet is about $7\times$ to $10\times$ faster than [3]. It should be noted that [3] was evaluated on a GTX Titan GPU which has 3072 CUDA cores and 12GB memory.

The non-dominated algorithms over running time and RMSE are shown in Fig. 6a. As can be seen, MobileXNet dominates Laina et al. [3] (UpConv), Laina et al. [3] (UpProj), Xu et al. [6] and Yang et al. [1]. Besides, MobileXNet, Wofk et al. [14] (Original), Wofk et al. [14] (Final) and Spek et al. [44] lie on the Pareto Front because none of them is dominated by another. Although MobileXNet is slower than [14] (Original), [14] (Final) and Spek et al. [44], its accuracy is much better than them. More importantly, MobileXNet runs about 126 fps on a less powerful GPU, which is adequate for the real-time application of autonomous driving and robotics. Considering the trade-off between accuracy and speed, MobileXNet is the best compromise solution. In Fig. 5, we provide qualitative comparison of the proposed method with [14], [25], [26]. It is clearly observed that the results of [14], [25], [26] are blurry. By contrast, our method recovers more details and the predicted depth maps are much clearer than its counterparts.

B. KITTI Dataset

The KITTI dataset [32] consists of outdoor scene images with a resolution of 375×1241 pixels. This dataset has sparse depth images captured by a Velodyne LiDAR. We utilize the same split as Eigen et al. [25], where only left images, which includes 22600 training images and 697 testing images are used. To generate the groundtruth depth maps, we projected corresponding Velodyne data points to the left image plane.

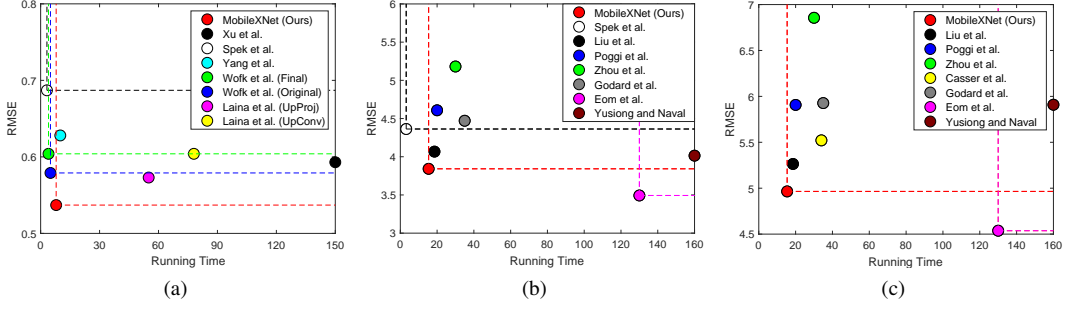


Fig. 6: Pareto Optimality. (a) The NYU depth v2 dataset, (b) The KITTI dataset (range caps of 50m), and (c) The KITTI dataset (range caps of 80m).

The missed depth values in the groundtruth depth maps are ignored both in training and testing. As the LiDAR provides no measurements in the upper part of the images, only the bottom 228×912 pixels region is used in this study.

In order to compare with state-of-the-art methods [2], [4], [5], [10], [25], [27], [44], [48]–[53], we evaluate our method with the depth ranging from 0m to 80m and 0m to 50m. Table VI shows the results of our method together with baselines. For the depth range from 0m to 80m, MobileXNet achieves the best REL and δ_3 results, while the value of RMSE is comparable to [2], [4]. Moreover, the δ_1 and δ_2 of MobileXNet are only slightly inferior to Cao et al. [4]. It should be noted that [4] is built on top of an extremely deep CNN, ResNet-152, and uses fully connected CRF for post-processing. In addition, Eom et al. [2] adopts a two-stream encoder in order to learn features from RGB image and optical flow. However, MobileXNet does not exploit any multi-stream architecture or post-processing operation, and has much less layers than [4]. In addition, our method outperforms [5], [10], [25], [48]–[53]. For the depth range of 0 to 50 meters, MobileXNet produced the best performance on REL, δ_2 , and δ_3 , and the second best performance of δ_1 . It demonstrates that MobileXNet works better for close-range depth.

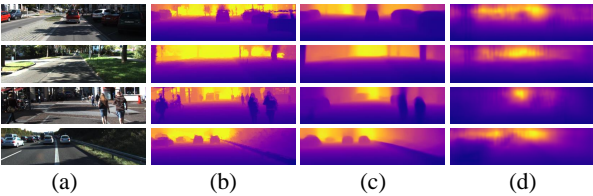


Fig. 7: Qualitative comparison on the KITTI dataset. (a) RGB, (b) Groundtruth, (c) Our results, and (d) Eigen et al. [25] (Fine). The groundtruth has been interpolated for visualization. Color represents depth (yellow is far, blue is close).

In terms of running speed, our MobileXNet only needs 15.4ms to process a 228×912 sized image on a GTX 1080 GPU, which is faster than its counterparts such as [2], [48]–[53]. It is worth noting that [2], [48]–[53] were tested on GPUs which are much stronger than ours. Specifically, the Titan-X GPU has 3584 CUDA cores and 12GB memory, the GTX 1080Ti GPU has 3584 CUDA cores and 11GB memory, while our GTX 1080 GPU only has 2560 CUDA cores and 8GB memory.

We use non-dominance to compare the running time and RMSE of the proposed MobileXNet, [2], [44], [48]–[53]. It can be observed from Fig. 6b and Fig. 6c that MobileXNet and Eom et al. [2] lie on the Pareto Front in the depth range between 0m and 80m. However, the MobileXNet is more than $8\times$ faster than Eom et al. [2], even though [2] was tested on a more powerful Titan-X GPU. As can be observed from Table VI, MobileXNet also outperforms Eom et al. [2] in REL, δ_1 , δ_2 , and δ_3 for depth range from 0m to 80m as well as 0m to 50m. According to the non-dominated set and Pareto front distribution, MobileXNet is the best solution among these methods. For the depth range of 0 to 50m, MobileXNet and Spek et al. [44] are non-dominated by each other. According to Table VI, the MobileXNet performs much better than Spek et al. [44] with respect to the error and accuracy metrics. Moreover, the MobileXNet achieves a real-time speed of 65 fps at a larger resolution (228×912 pixels). Hence, MobileXNet is the best solution among these methods. Qualitative results are shown in Fig. 7. As can be observed, our method generates much clearer depth maps than [25].

According to [48], [56], the depth measurements from the LiDAR may be influenced by many factors such as rotation of the LiDAR and incorrect depth readings resulting from the occlusion at object boundaries. In order to better validate the performance of our proposed MobileXNet, we applied the same split of images with more accurate groundtruth labels provided by the KITTI official [56]. The annotated depth maps are generated by filtering LiDAR points with a computed disparity map from the Semi-Global Matching algorithm [57] to remove outliers from the raw measurements. It is worth noting that the annotated depth maps are not available for 315 training and 45 testing images of the original Eigen split, thus, the number of training and testing images are 22 285 and 652 respectively. The missed values in the annotated depth maps are ignored during both training and evaluation.

We compare our method with [48], [54], [55]. The results of [48] and [55] are reported in [55]. Quantitative results are listed in Table VII. As shown in rows 1 to 4 of Table VII, for the cap of 0-80m, MobileXNet outperforms all baselines in terms of REL, δ_1 , δ_2 and δ_3 , while the RMSE is slightly inferior to [54]. It is worth noting that [54] applies ResNet-50 as encoder, which is much deeper than the network of MobileXNet. Since [54] only reports results in the range of 0-80m, thus, we compare MobileXNet with [48] and [55] for the cap of 0-50m. It can be seen from rows 5 to 7 of Table VII, with a simple and shallow network architecture the proposed

TABLE VII: Comparison of performances on 93.5% of the KITTI Eigen-split with accurate groundtruth labels released by the KITTI evaluation benchmark. K denotes the KITTI dataset, CS refers to the Cityscapes dataset, CS + K represents training on the Cityscapes dataset then fine-tuning on the KITTI dataset. \triangle represents the first 9 layers of MobileNet. The **red** and **bold** values indicate the best results.

Row	Method	Cap	Backbone	Dataset	RMSE	REL	δ_1	δ_2	δ_3
1	Amiri et al. [54]	80 m	ResNet-50	K	3.995	0.096	0.892	0.972	0.992
2	Godard et al. [48]	80 m	ResNet-50	CS+K	4.279	0.097	0.898	0.973	0.991
3	Aleotti et al. [55]	80 m	VGG-16	CS+K	4.236	0.096	0.899	0.974	0.992
4	MobileXNet (Ours)	80 m	\triangle	K	4.128	0.087	0.905	0.976	0.993
5	Godard et al. [48]	50 m	ResNet-50	CS+K	4.100	0.095	0.896	0.975	0.992
6	Aleotti et al. [55]	50 m	VGG-16	CS+K	4.110	0.094	0.897	0.976	0.993
7	MobileXNet (Ours)	50 m	\triangle	K	3.081	0.083	0.916	0.981	0.994
		Lower is better	Higher is better	$\delta_1 : \delta < 1.25, \delta_2 : \delta < 1.25^2, \delta_3 : \delta < 1.25^3$					

MobileXNet outperforms [48] and [55] in all metrics.

C. Make 3D Dataset

In this part, we evaluate MobileXNet on the Make3D dataset [12], consisting of 400 training and 134 testing images. The RGB images have a resolution of 2272×1704 pixels, and the corresponding groundtruth depth map is 55×305 sized. Following [58] all images are downsampled to 568×426 pixels. In this study, we train our network on the 460×345 pixels center cropped region. To compare with the state-of-the-art, we evaluate the trained model with C1 (depth range from 0m to 70m) and C2 (depth range from 0m to 80m) criterions as introduced in [24].

TABLE VIII: Qualitative results on the Make3D dataset. The **red** and **bold** values indicate the best results.

Method	C1 error			C2 error		
	REL	log10	RMSE	REL	log10	RMSE
Liu et al. [24]	0.335	0.137	9.49	0.338	0.134	12.60
Karsch et al. [13]	0.355	0.127	9.20	0.361	0.148	15.10
Li et al. [59]	0.278	0.092	7.12	0.279	0.102	10.27
Liu et al. [27]	0.287	0.109	7.36	0.287	0.122	14.09
Roy and Todorovic [60]	N/A	N/A	N/A	0.260	0.119	12.40
Godard et al. [48]	0.443	0.143	8.860	N/A	N/A	N/A
Kuznetsov et al. [61]	0.421	0.190	8.24	N/A	N/A	N/A
Fu et al. [58]	0.236	0.082	7.02	0.238	0.087	10.01
Zhao et al. [62]	0.403	N/A	10.424	N/A	N/A	N/A
MobileXNet (Ours)	0.229	0.086	6.807	0.233	0.089	8.020
		Lower is better				

The previous methods [13], [24], [27], [48], [58]–[62] are used as baseline, all results are shown in Table VIII. As can be observed, MobileXNet outperforms [13], [24], [27], [48], [59]–[62] in all metrics. As for [58], our method generates better REL and RMSE results, while the log10 value is slightly inferior. It is worth noting that [58] applies a deep CNN as backbone and combines a scene understanding module. In addition, our MobileXNet only needs 0.012s to compute a depth map on a single GTX 1080 GPU. For Liu et al. [27], 1.1s is required to infer depth map from a test image. However, the time for computing superpixels is not included. Qualitative results from this dataset are shown in Fig. 8.

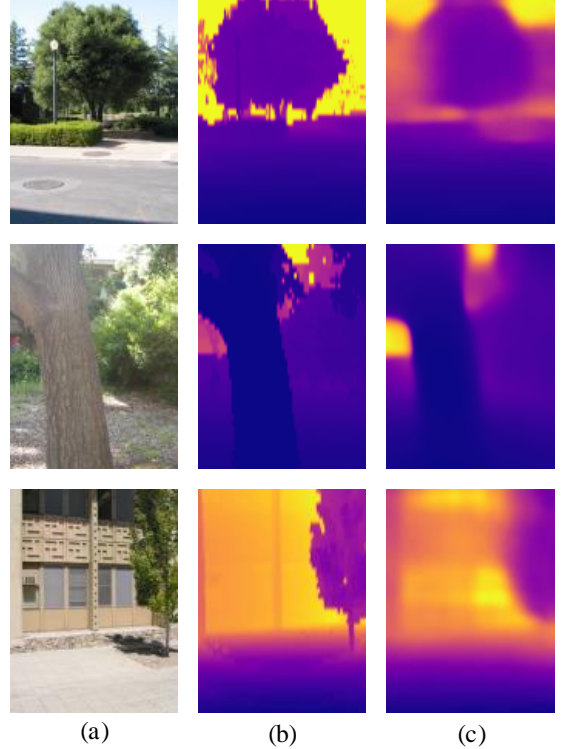


Fig. 8: Quantitative results on the Make3D dataset. (a) RGB, (b) Groundtruth, and (c) Our results. Color represents depth (yellow is far, blue is close).

D. UnrealDataset

To demonstrate the ability of predicting depth maps from small sized images, we evaluate the proposed MobileXNet on the UnrealDataset [33]. This data set contains over 100K images collected in a series of simulated urban and forest scenarios, and the groundtruth depth up to 40 meters. Compared with the aforementioned data sets [12], [31], [32], the RGB and depth images in the UnrealDataset have a much smaller size, 160×256 pixels. The Unreal Engine and AirSim softwares simulate an MAV flying in the simulated environments. The RGB and depth image pairs are collected from the MAV's frontal camera using a plugin. We first evaluate the proposed method on original images, and compare it with [7], [14], [33], [40]. Considering the limitation of GPU memory, we

choose the ResNet50-DeConv3³ combination of [7]. We train [7], [14] with the official released source code and default parameters. As in section V, we train the Pytorch implemented U-Net (Bilinear) with the hybrid loss function.

From rows 1 to 5 of Table IX, we show the quantitative comparison between MobileXNet and baselines on the original images. Following [33], we only report the RMSE and running time of J-MOD2. As can be observed, MobileXNet outperforms [7], [14] in all metrics. It performs best in REL, δ_3 and speed, while the RMSE value of MobileXNet is slightly inferior to J-MOD2. J-MOD2 is a multi-task learning method, which jointly learns object detection and depth estimation. The object detection branch informs the depth estimation branch with object structures, which improves the accuracy of depth estimation. However, our method only works out MDE. According to Fig. 11a, both MobileXNet and J-MOD2 are non-dominated solutions. The running time of J-MOD2 is longer than MobileXNet, even though J-MOD2 was evaluated on a more powerful GPU. The threshold metric of MobileXNet is on par with U-Net [40]. It is worth noting that images from the UnrealDataset are much smaller than the NYU v2 dataset [31]. As both U-Net and MobileXNet downsample the feature maps to 1/16 scale of the input images, the produced feature maps include more spatial information than [7], [14]. In addition, U-Net [40] is twice as wide as our MobileXNet, which enables U-Net to learn more information. Some qualitative results of our method and baselines are shown in Fig. 9, which further demonstrates the superior performance of MobileXNet.

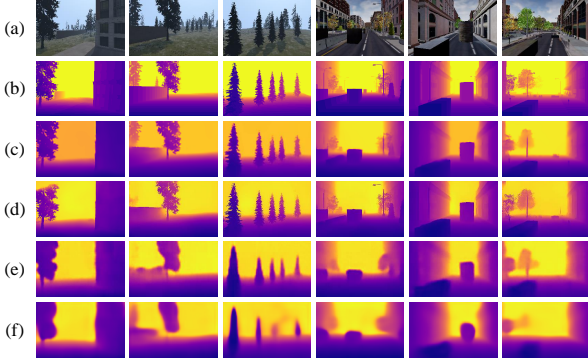


Fig. 9: Qualitative comparison on the UnrealDataset (original). (a) RGB, (b) Groundtruth, (c) Our results, (d) U-Net [40], (e) Ma and Karaman [7], and (f) Wofk et al. [14] (Original). Color represents depth (yellow is far, blue is close).

To further validate the ability of MobileXNet to process small sized images, we downsample the original images to 128×204 and 80×128 pixels. We compare our method with [7], [14], [40]. The rows 6 to 9 and rows 10 to 15 of Table IX show results on 128×204 and 80×128 sized images respectively. It can be observed that reducing the image size decreases the performance of depth estimation. It is worth noting that when images are downsampled to 80×128 pixels, the performance of Ma and Karaman [7] dropped significantly. Ma and Karaman [7] use the fully convolutional part of ResNet-50 as encoder. Besides the inherent characteristic of

³The fully convolutional part of ResNet-50 is used as the encoder and the deconvolution with 3×3 kernel is applied for upsampling.

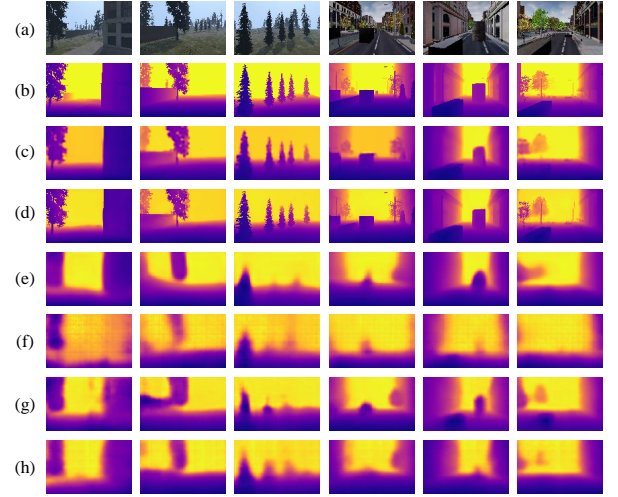


Fig. 10: Qualitative comparison on the UnrealDataset (80×128). (a) RGB, (b) Groundtruth, (c) Our results, (d) U-Net [40], (e) Wofk et al. [14] (Original), (f) Ma and Karaman [7], (g) Ma and Karaman [7] with 5×5 sized filters in the input layer, and (h) Ma and Karaman [7] with 3×3 sized filters in the input layer. Color represents depth (yellow is far, blue is close).

the encoder network, the 7×7 sized filters in the input layer may have influence on the performance. For small sized images, large filters could capture global information, while the detail information are missed. Unlike image classification, depth estimation is a pixel-wise application, both global and detailed information are important. Our hypothesis is that using smaller sized filters in the input layer will help to improve the performance of Ma and Karaman [7]. As a result, we modified [7] by reducing the filter kernel size in the input layer from 7 to 5 and 3 respectively.

It can be observed from rows 11 to 13 of Table VII, both 5×5 and 3×3 sized filter-based input layers improve the performance of Ma and Karaman [7]. We present a qualitative comparison between our method and baselines in Fig. 10. It is clear that the modified Ma and Karaman [7] with small sized filter-based input layers performs better than the original. Thus, we can conclude that the input layer with small sized filters is helpful in predicting depth from small sized images. It is worth noting that MobileXNet outperforms the modified Ma and Karaman [7] in all metrics and generates much clearer depth maps, although the latter has a very deep encoder network. Moreover, according to Fig. 11b and c, the proposed MobileXNet is the non-dominated solution in 128×204 and 80×128 sized images. This demonstrates the superior performance of MobileXNet on small sized images.

VI. CONCLUSIONS AND FUTURE WORK

In this paper, we paid attention to the trade-off between the accuracy and speed of monocular depth estimation (MDE). To this end, we introduced a novel and real-time CNN architecture, namely, MobileXNet. By assembling two shallow and simple encoder-decoder subnetworks back-to-back in a unified framework, MobileXNet utilizes a simple network architecture and avoids a greater number of successive downsamplings. With the benefit of this design, the proposed method

TABLE IX: Comparison of performances on the UnrealDataset. \diamond means the network does not use CNN designed for image classification, \triangle represents the first 9 layers of MobileNet. Ma and Karaman (3×3) and Ma and Karaman (5×5) denote the use of 3×3 and 5×5 sized filters in the input layer respectively. The **red** and **bold** values indicate the best results.

Row	Method	Backbone	Input Size	RMSE	REL	δ_1	δ_2	δ_3	t_{GPU}	Device
1	J-MOD2 [33]	VGG-19	160×256	3.473	N/A	N/A	N/A	N/A	10 ms	Nvidia Titan-X
2	U-Net [40]	\diamond	160×256	3.834	0.130	0.884	0.957	0.977	8.8 ms	Nvidia GTX 1080
3	Ma and Karaman [7]	ResNet-50	160×256	4.023	0.126	0.870	0.951	0.974	6.9 ms	Nvidia GTX 1080
4	Wofk et al. [14]	MobileNet	160×256	4.208	0.155	0.860	0.945	0.972	6.7 ms	Nvidia GTX 1080
5	MobileXNet (Ours)	\triangle	160×256	3.612	0.124	0.878	0.954	0.977	6.6 ms	Nvidia GTX 1080
6	U-Net [40]	\diamond	128×204	3.917	0.134	0.879	0.956	0.969	6.9 ms	Nvidia GTX 1080
7	Ma and Karaman [7]	ResNet-50	128×204	4.188	0.138	0.856	0.946	0.973	6.6 ms	Nvidia GTX 1080
8	Wofk et al. [14]	MobileNet	128×204	4.393	0.157	0.852	0.940	0.976	6.4 ms	Nvidia GTX 1080
9	MobileXNet (Ours)	\triangle	128×204	3.733	0.133	0.871	0.954	0.977	6.3 ms	Nvidia GTX 1080
10	U-Net [40]	\diamond	80×128	3.912	0.135	0.873	0.956	0.977	4.8 ms	Nvidia GTX 1080
11	Ma and Karaman [7]	ResNet-50	80×128	8.399	0.444	0.511	0.681	0.868	5.8 ms	Nvidia GTX 1080
12	Ma and Karaman (5×5) [7]	ResNet-50	80×128	4.988	0.178	0.798	0.923	0.962	6.7 ms	Nvidia GTX 1080
13	Ma and Karaman (3×3) [7]	ResNet-50	80×128	4.744	0.174	0.804	0.930	0.967	6.7 ms	Nvidia GTX 1080
14	Wofk et al. [14]	MobileNet	80×128	4.874	0.166	0.814	0.928	0.967	7.3 ms	Nvidia GTX 1080
15	MobileXNet (Ours)	\triangle	80×128	3.904	0.140	0.853	0.948	0.975	5.8 ms	Nvidia GTX 1080
				Lower is better	Higher is better	$\delta_1 : \delta < 1.25, \delta_2 : \delta < 1.25^2, \delta_3 : \delta < 1.25^3$				

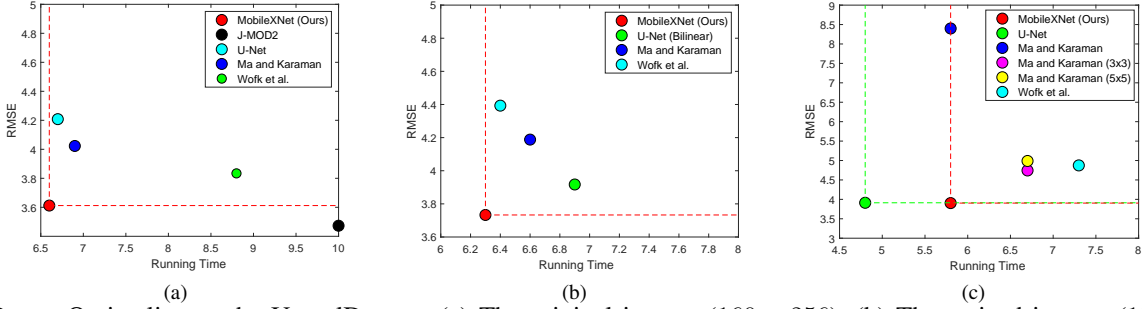


Fig. 11: Pareto Optimality on the UnrealDataset. (a) The original images (160×256), (b) The resized images (128×204), and (c) The resized images (80×128).

not only achieve a proper trade-off between the accuracy and speed of MDE, but also shows superior performance on the small sized images. Being designed in the encoder-decoder style and trained in the end-to-end manner, the proposed network also can be transferred to other applications, e.g., foreground segmentation [63].

We also designed a hybrid loss function by employing an additional spatial derivative-based L_1 loss function together with the regular L_1 function. Comprehensive experiments have been conducted on the NYU depth v2, KITTI, Make3D and Unreal data sets. Experimental results showed that the proposed method performed comparably to the state-of-the-art methods which either were implemented with a complex and extremely deep architecture or used post-processing. More importantly, the proposed MobileXNet run at a much faster speed on a single less powerful GPU, which is particularly critical for real-time autonomous driving and robotic applications.

In the future, we will investigate more light-weight and accurate variants of the MobileXNet network and apply it to obstacle avoidance of MAVs.

REFERENCES

- [1] X. Yang, J. Chen, Y. Dang, H. Luo, Y. Tang, C. Liao, P. Chen, and K.-T. Cheng, "Fast depth prediction and obstacle avoidance on a monocular drone using probabilistic convolutional neural network," *IEEE TITS*, 2019.
- [2] C. Eom, H. Park, and B. Ham, "Temporally consistent depth prediction with flow-guided memory units," *IEEE TITS*, vol. 21, no. 11, pp. 4626–4636, 2020.
- [3] I. Laina, C. Rupprecht, V. Belagiannis, F. Tombari, and N. Navab, "Deeper depth prediction with fully convolutional residual networks," in *3DV*, 2016, pp. 239–248.
- [4] Y. Cao, Z. Wu, and C. Shen, "Estimating depth from monocular images as classification using deep fully convolutional residual networks," *IEEE TCSVT*, vol. 28, no. 11, pp. 3174–3182, 2017.
- [5] B. Li, Y. Dai, and M. He, "Monocular depth estimation with hierarchical fusion of dilated CNNs and soft-weighted-sum inference," *PR*, vol. 83, pp. 328–339, 2018.
- [6] D. Xu, W. Wang, H. Tang, H. Liu, N. Sebe, and E. Ricci, "Structured attention guided convolutional neural fields for monocular depth estimation," in *CVPR*, 2018, pp. 3917–3925.
- [7] F. Ma and S. Karaman, "Sparse-to-dense: Depth prediction from sparse depth samples and a single image," in *ICRA*, 2018, pp. 4796–4803.
- [8] J. Hu, M. Ozay, Y. Zhang, and T. Okatani, "Revisiting single image depth estimation: Toward higher resolution maps with accurate object boundaries," in *WACV*, 2019, pp. 1043–1051.
- [9] X. Chen, X. Chen, and Z.-J. Zha, "Structure-aware residual pyramid network for monocular depth estimation," *arXiv preprint arXiv:1907.06023*, 2019.
- [10] X. Ye, S. Chen, and R. Xu, "DPNet: Detail-preserving network for high quality monocular depth estimation," *PR*, p. 107578, 2020.
- [11] A. Saxena, S. H. Chung, and A. Y. Ng, "Learning depth from single monocular images," in *NIPS*, 2006, pp. 1161–1168.
- [12] A. Saxena, M. Sun, and A. Y. Ng, "Make3D: Learning 3D scene structure from a single still image," *IEEE TPAMI*, vol. 31, no. 5, pp. 824–840, 2008.

- [13] K. Karsch, C. Liu, and S. B. Kang, "Depth transfer: Depth extraction from video using non-parametric sampling," *IEEE TPAMI*, vol. 36, no. 11, pp. 2144–2158, 2014.
- [14] D. Wofk, F. Ma, T.-J. Yang, S. Karaman, and V. Sze, "FastDepth: Fast monocular depth estimation on embedded systems," in *ICRA*, 2019, pp. 6101–6108.
- [15] A. G. Howard, M. Zhu, B. Chen, D. Kalenichenko, W. Wang, T. Weyand, M. Andreetto, and H. Adam, "MobileNets: Efficient convolutional neural networks for mobile vision applications," *arXiv preprint arXiv:1704.04861*, 2017.
- [16] T.-J. Yang, A. Howard, B. Chen, X. Zhang, A. Go, M. Sandler, V. Sze, and H. Adam, "NetAdapt: Platform-aware neural network adaptation for mobile applications," in *ECCV*, 2018, pp. 285–300.
- [17] K. He, X. Zhang, S. Ren, and J. Sun, "Deep residual learning for image recognition," in *CVPR*, 2016, pp. 770–778.
- [18] G. Huang, Z. Liu, L. Van Der Maaten, and K. Q. Weinberger, "Densely connected convolutional networks," in *CVPR*, 2017, pp. 4700–4708.
- [19] J. Hu, L. Shen, and G. Sun, "Squeeze-and-excitation networks," in *CVPR*, 2018, pp. 7132–7141.
- [20] C. Szegedy, W. Liu, Y. Jia, P. Sermanet, S. Reed, D. Anguelov, D. Erhan, V. Vanhoucke, and A. Rabinovich, "Going deeper with convolutions," in *CVPR*, 2015, pp. 1–9.
- [21] J. Bullock, C. Cuesta-Lázaro, and A. Quera-Bofarull, "XNet: A convolutional neural network (CNN) implementation for medical X-Ray image segmentation suitable for small datasets," in *Medical Imaging 2019: Biomedical Applications in Molecular, Structural, and Functional Imaging*, vol. 10953, 2019, p. 109531Z.
- [22] F. Chollet, "Xception: Deep learning with depthwise separable convolutions," in *CVPR*, 2017, pp. 1251–1258.
- [23] B. Liu, S. Gould, and D. Koller, "Single image depth estimation from predicted semantic labels," in *CVPR*, 2010, pp. 1253–1260.
- [24] M. Liu, M. Salzmann, and X. He, "Discrete-continuous depth estimation from a single image," in *CVPR*, 2014, pp. 716–723.
- [25] D. Eigen, C. Puhrsch, and R. Fergus, "Depth map prediction from a single image using a multi-scale deep network," in *NIPS*, 2014, pp. 2366–2374.
- [26] D. Eigen and R. Fergus, "Predicting depth, surface normals and semantic labels with a common multi-scale convolutional architecture," in *ICCV*, 2015, pp. 2650–2658.
- [27] F. Liu, C. Shen, G. Lin, and I. Reid, "Learning depth from single monocular images using deep convolutional neural fields," *IEEE TPAMI*, vol. 38, no. 10, pp. 2024–2039, 2015.
- [28] K. Zhou, K. Wang, and K. Yang, "PADENet: An efficient and robust panoramic monocular depth estimation network for outdoor scenes," in *ITSC*, 2020, pp. 1–6.
- [29] K. Yang, X. Hu, Y. Fang, K. Wang, and R. Stiefelhagen, "Omnisuper-vised omnidirectional semantic segmentation," *IEEE TITS*, 2020.
- [30] Y. Liu, C. Shu, J. Wang, and C. Shen, "Structured knowledge distillation for dense prediction," *IEEE TPAMI*, 2020.
- [31] N. Silberman, D. Hoiem, P. Kohli, and R. Fergus, "Indoor segmentation and support inference from RGB-D images," in *ECCV*, 2012, pp. 746–760.
- [32] A. Geiger, P. Lenz, C. Stiller, and R. Urtasun, "Vision meets robotics: The KITTI dataset," *IJRR*, vol. 32, no. 11, pp. 1231–1237, 2013.
- [33] M. Mancini, G. Costante, P. Valigi, and T. A. Ciarfuglia, "J-MOD 2: Joint monocular obstacle detection and depth estimation," *IEEE RAL*, vol. 3, no. 3, pp. 1490–1497, 2018.
- [34] O. Russakovsky, J. Deng, H. Su, J. Krause, S. Satheesh, S. Ma, Z. Huang, A. Karpathy, A. Khosla, M. Bernstein *et al.*, "ImageNet large scale visual recognition challenge," *IJCV*, vol. 115, no. 3, pp. 211–252, 2015.
- [35] F. Yu and V. Koltun, "Multi-scale context aggregation by dilated convolutions," *arXiv preprint arXiv:1511.07122*, 2015.
- [36] Z. Wojna, V. Ferrari, S. Guadarrama, N. Silberman, L.-C. Chen, A. Fathi, and J. Uijlings, "The devil is in the decoder: classification, regression and GANs," *IJCV*, vol. 127, no. 11–12, pp. 1694–1706, 2019.
- [37] G. Irie, T. Kawanishi, and K. Kashino, "Robust learning for deep monocular depth estimation," in *ICIP*, 2019, pp. 964–968.
- [38] S. Kumari, R. R. Jha, A. Bhavsar, and A. Nigam, "AutoDepth: Single image depth map estimation via residual CNN encoder-decoder and stacked hourglass," in *ICIP*, 2019, pp. 340–344.
- [39] J. Jiao, Y. Cao, Y. Song, and R. Lau, "Look deeper into depth: Monocular depth estimation with semantic booster and attention-driven loss," in *ECCV*, 2018, pp. 53–69.
- [40] O. Ronneberger, P. Fischer, and T. Brox, "U-Net: Convolutional networks for biomedical image segmentation," in *ICMICI*, 2015, pp. 234–241.
- [41] X. Dong, C. J. Taylor, and T. F. Cootes, "Defect detection and classification by training a generic convolutional neural network encoder," *IEEE TSP*, vol. 68, pp. 6055–6069, 2020.
- [42] L. He, G. Wang, and Z. Hu, "Learning depth from single images with deep neural network embedding focal length," *TIP*, vol. 27, no. 9, pp. 4676–4689, 2018.
- [43] P. Hambarde and S. Murala, "S2DNet: Depth estimation from single image and sparse samples," *IEEE TCI*, 2020.
- [44] A. Spek, T. Dharmasiri, and T. Drummond, "CReaM: Condensed real-time models for depth prediction using convolutional neural networks," in *IROS*, 2018, pp. 540–547.
- [45] N. Ma, X. Zhang, H.-T. Zheng, and J. Sun, "ShuffleNet V2: Practical guidelines for efficient CNN architecture design," in *ECCV*, 2018, pp. 116–131.
- [46] M. Tan and Q. Le, "EfficientNet: Rethinking model scaling for convolutional neural networks," in *ICML*, 2019, pp. 6105–6114.
- [47] I. Radosavovic, R. P. Kosaraju, R. Girshick, K. He, and P. Dollár, "Designing network design spaces," in *CVPR*, 2020, pp. 10428–10436.
- [48] C. Godard, O. Mac Aodha, and G. J. Brostow, "Unsupervised monocular depth estimation with left-right consistency," in *CVPR*, 2017, pp. 270–279.
- [49] T. Zhou, M. Brown, N. Snavely, and D. G. Lowe, "Unsupervised learning of depth and ego-motion from video," in *CVPR*, 2017, pp. 1851–1858.
- [50] M. Poggi, F. Aleotti, F. Tosi, and S. Mattocchia, "Towards real-time unsupervised monocular depth estimation on CPU," in *IROS*, 2018, pp. 5848–5854.
- [51] V. Casser, S. Pirk, R. Mahjourian, and A. Angelova, "Depth prediction without the sensors: Leveraging structure for unsupervised learning from monocular videos," in *AAAI*, vol. 33, 2019, pp. 8001–8008.
- [52] J. P. Yusiong and P. Naval, "AsiANet: Autoencoders in autoencoder for unsupervised monocular depth estimation," in *WACV*, 2019, pp. 443–451.
- [53] J. Liu, Q. Li, R. Cao, W. Tang, and G. Qiu, "MiniNet: An extremely lightweight convolutional neural network for real-time unsupervised monocular depth estimation," *ISPRS JPRS*, vol. 166, pp. 255–267, 2020.
- [54] A. J. Amiri, S. Y. Loo, and H. Zhang, "Semi-supervised monocular depth estimation with left-right consistency using deep neural network," in *ROBIO*, 2019, pp. 602–607.
- [55] F. Aleotti, F. Tosi, M. Poggi, and S. Mattocchia, "Generative adversarial networks for unsupervised monocular depth prediction," in *ECCV Workshops*, 2018, pp. 337–354.
- [56] J. Uhrig, N. Schneider, L. Schneider, U. Franke, T. Brox, and A. Geiger, "Sparsity invariant CNNs," in *3DV*, 2017, pp. 11–20.
- [57] H. Hirschmüller, "Stereo processing by semiglobal matching and mutual information," *IEEE TPAMI*, vol. 30, no. 2, pp. 328–341, 2007.
- [58] H. Fu, M. Gong, C. Wang, K. Batmanghelich, and D. Tao, "Deep ordinal regression network for monocular depth estimation," in *CVPR*, 2018, pp. 2002–2011.
- [59] B. Li, C. Shen, Y. Dai, A. Van Den Hengel, and M. He, "Depth and surface normal estimation from monocular images using regression on deep features and hierarchical CRFs," in *CVPR*, 2015, pp. 1119–1127.
- [60] A. Roy and S. Todorovic, "Monocular depth estimation using neural regression forest," in *CVPR*, 2016, pp. 5506–5514.
- [61] Y. Kuznetsov, J. Stuckler, and B. Leibe, "Semi-supervised deep learning for monocular depth map prediction," in *CVPR*, 2017, pp. 6647–6655.
- [62] S. Zhao, H. Fu, M. Gong, and D. Tao, "Geometry-aware symmetric domain adaptation for monocular depth estimation," in *CVPR*, 2019, pp. 9788–9798.
- [63] T. Akilan, Q. J. Wu, A. Safaei, J. Huo, and Y. Yang, "A 3D CNN-LSTM-based image-to-image foreground segmentation," *IEEE TITS*, vol. 21, no. 3, pp. 959–971, 2019.